

Temporal laser pulse shape effects in nonlinear Thomson scattering

V. Yu. Kharin* and S. G. Rykovanov

Helmholtz-Institut Jena, Fröbelstieg 3, 07743 Jena, Germany

D. Seipt

Friedrich-Schiller-Universität, Theoretisch Physikalisches Institut, 07743, Jena, Germany

(Dated: February 10, 2016)

Abstract

The influence of the laser pulse temporal shape on the Nonlinear Thomson Scattering on-axis photon spectrum is analyzed in detail. Using the classical description, analytical expressions for the temporal and spectral structure of the scattered radiation are obtained for the case of symmetric laser pulse shapes. The possibility of reconstructing the incident laser pulse from the scattered spectrum averaged over interference fringes in the case of high peak intensity and symmetric laser pulse shape is discussed.

* v.kharin@gsi.de

I. INTRODUCTION

During the last decades scattering of light on high-energy electron beams has become an indispensable tool for generating tunable wide range X- and γ -radiation[1–8]. These Thomson scattering (TS) sources have found applications in spectroscopy[9–12], medicine[13], ultrafast radiography[14, 15], and nuclear nonproliferation[16–18]. The conversion of laser photons to γ -radiation occurs as the Doppler upshift of the laser frequency while scattering on electrons with high gamma-factor. Since the TS cross-section is relatively small, for the generation of bright X- and γ -ray beams one benefits from employing high-intensity incident laser pulses. However, the longitudinal drift of the electron in the strong wave – caused by the $\mathbf{v} \times \mathbf{B}$ force – results in significant shift of the radiation frequency. This gives rise to the broadening of the spectral components of the scattered light and a specific interference structure inside each spectral harmonic[19–25]. A number of recent works were devoted to the studies of such a ponderomotive broadening, and its compensation by the usage of laser chirping techniques[25–28]. However, a quantitative analytical description of the nonlinear TS still remains an open question.

In this paper, the temporal and spectral structure of the on-axis scattered radiation for nonlinear TS is found analytically within the assumption of a symmetric laser pulse temporal shape for both linear and circular laser pulse polarization. It is demonstrated that the shape of the envelope of the scattered spectrum permits the reconstruction of the temporal structure of the strong incident laser pulse. This could be useful for intense laser-matter interaction experiments.

The paper is organized as follows. In Sec. II the analytical description of the nonlinear Thomson back-scattering is provided within classical electrodynamics. That means, equations of motion for electron are solved, and the scattered radiation is calculated using Lienard-Wiechert potentials. The detector time consideration described in this section provides also an efficient way of calculating the scattered spectrum numerically. This is covered in Sect. III, where we provide the details of a fast numerical routine for evaluation of the back-scattered spectrum. Subsect. IIIB contains the scattered spectra for various laser pulse shapes. The details of the scattered pulse formation in time domain allow us to make qualitative statements about the spectrum. The shape of the back-scattered spectrum can be evaluated analytically with good accuracy. Using this approach, one sees that the shapes

of the scattered light spectra at relatively high intensity differ a lot, even when the envelope profile difference is not very well pronounced. It is shown, that in case of the symmetric pulse envelope and high peak intensity one can reconstruct the incident pulse envelope profile without resolving the interference structure of the nonlinear TS. In the conclusions (Sect. IV) the results are summed up, and the possible influence of the effects not included in the model is discussed. An Appendix contains derivation of the scattered spectral intensity in case of linearly polarized pulse and shapes of spectral intensity profiles for the pulses used in the article

II. ANALYTICAL DESCRIPTION

Throughout the paper the classical description of TS process is used. That is, the classical equations of motion of the electron are solved, and the scattered field is calculated using Lienard-Wiechert[29, 30] potentials. Within this framework the electron recoil is assumed negligible. For this case the structure of integrals defining spectral intensity remains similar to the one in the first order perturbation theory in quantum electrodynamical framework (cf. [23, 31] and [25]). Despite the simplicity of the underlying model, even the scattering of quasi-monochromatic plane wave radiation demonstrates a rich physics, as will be shown further.

The influence of spin effects on the scattered spectra and comparison between classical and QED solutions can be found in [32, 33]. Both the classical and quantum mechanical approaches mentioned above use the approximation that the strong incident laser pulse is described as a purely classical. Description of the strong-field dynamics in quantized external field is another complicated and interesting problem.

A. General setup

Throughout the paper the natural units for the relativistic kinematics in the laser field are adopted. In these dimensionless units

$$t = \omega_L \hat{t}, \quad x = k_L \hat{x}, \quad y = k_L \hat{y}, \quad z = k_L \hat{z}, \quad A = \frac{e \hat{A}}{m_e c^2},$$

where the “hatted” values are given in Gaussian CGS units, t , x , y and z are the natural time and coordinates, A is the normalized vector potential, e and m_e are the electron absolute

charge and mass, respectively, c is the speed of light in vacuum, ω_L is the central laser pulse frequency, and $k_L = \omega_L/c$.

Since one can always apply the Lorentz transformation to the electron frame of reference, we consider the electron initially at rest keeping in mind that for real situation the calculated spectra should be Lorentz transformed back. It should be mentioned, that in this frame of reference the scattered light will not be Doppler up-shifted because the initial gamma-factor of the electron is 1. We also constrain ourselves to the case of the on-axis scattering. The equations of motion for the charged particle in the plane wave field can be solved analytically[34]. One can choose the gauge where the vector potential \mathbf{A}^L of the laser is transverse (i.e., it has only x and y components), and the wave is propagating in z direction:

$$\mathbf{A}^L = \mathbf{A}^L(t - z). \quad (1)$$

Superscript L stands for “laser” (not to confuse the laser field with the vector potential \mathbf{A} describing the scattered field). We use the notation $\varphi = t - z$ for the laser pulse phase, $\zeta = t + z$. Moreover, we require that the laser vector potential vanishes asymptotically, $\mathbf{A}^L \rightarrow 0$ at $\varphi \rightarrow \pm\infty$. The analytic solution of the equations of motion for components of electron four-velocity u reads

$$\gamma - u_z = 1, \quad (2)$$

$$u_{x,y} = A_{x,y}^L, \quad (3)$$

$$\gamma + u_z = 1 + |\mathbf{A}^L|^2, \quad (4)$$

$$\zeta = \varphi + \int_0^\varphi |\mathbf{A}^L(\xi)|^2 d\xi, \quad (5)$$

where γ is the Lorentz factor of the electron. As there is no significant difference between the x and y components of the scattered radiation, one can work with only one component (x , for example). The Lienard-Wiechert formula for the vector potential of the back-scattered light that arrives at the distance R from the initial electron position at time t can be written as follows

$$A_x(t) = \frac{1}{R - z} \frac{u_x}{\gamma + u_z} \bigg|_{t_{ret}}, \quad (6)$$

where t_{ret} is the retarded time when the light wave was emitted by the electron. As the far-field distribution of the radiation is the subject of interest, one can omit the change in the electron position z in the denominator, since it contributes only to terms decreasing

faster than $1/R$ with $|z| \ll R$. Hence, the following relation between the retarded time t_{ret} and the detector time t can be written:

$$t = R + z(t_{ret}) + t_{ret}. \quad (7)$$

If one now tunes the detector clock to the delay, $t \mapsto t + R$, one can immediately see that the detector time is exactly equal to the variable ζ defined above. Since the explicit solution of the electron equation of motion, Eqs. (2-5), is written in terms of the pulse phase φ , and there is the expression for ζ , it is convenient to eliminate the t_{ret} dependence, and get the expression for the vector potential of the emitted radiation as

$$\mathbf{A}(\zeta) = \frac{1}{R} \frac{\mathbf{A}^L(\varphi(\zeta))}{1 + |\mathbf{A}^L(\varphi(\zeta))|^2}. \quad (8)$$

Here the variable ζ is precisely the detector time shifted by the constant value of R , and the dependence $\varphi(\zeta)$ is given implicitly by (5). Taking the Fourier transform of (8) with respect to detector time and changing the variables of integration from ζ to φ yields the following simple expression for the spectrum of \mathbf{A} :

$$\mathbf{A}(\omega) = \frac{1}{R} \int_{-\infty}^{+\infty} \mathbf{A}^L(\varphi) e^{i\omega\zeta} d\varphi. \quad (9)$$

Both the cases of circularly and linearly polarized intense laser light with slowly varying amplitude can be considered to provide the analytical description of the back-scattered radiation spectrum.

B. Circular polarization

Let us start with the case of circular laser polarization, since, as we shall see soon, this simplifies the analytical expressions. We take the pulse in the following form

$$A_x^L(\varphi) = a(\varphi) \cos \varphi, \quad (10)$$

$$A_y^L(\varphi) = a(\varphi) \sin \varphi, \quad (11)$$

where $a(\varphi)$ is a slowly varying amplitude. With this laser vector potential Eq. (5) can be written as

$$\zeta = \varphi + \int_0^\varphi a(\xi)^2 d\xi, \quad (12)$$

where the non-linear term depends only on the envelope of the vector potential $a(\varphi)$, and there are no oscillations (with the frequency of the order of unity) in it. Physically, this leads to the absence of high order harmonics in the on-axis back-scattered radiation[35]. One can consider only one component of the scattered field, since the reasoning for the other component (and the spectra) will be the same. We rewrite the scattered vector potential in terms of $a(\varphi)$ as

$$A_x(\zeta) = \frac{1}{R} \frac{a(\varphi(\zeta))}{1 + a(\varphi(\zeta))^2} \cos \varphi(\zeta), \quad (13)$$

From now on we will refer to a_0 as the peak value of $a(\varphi)$. The argument of the instant amplitude dependence $a(\varphi)$ will be omitted when it cannot lead to confusion. From (13) one can clearly see that if $a_0 \ll 1$ the scattered pulse reproduces the incident one, $A_x(\zeta) = A_x^L(\zeta)/R$, because $\zeta \approx \varphi$. When a_0 increases, two effects contributing to the scattered pulse modification can be noticed. The first one is due to the nontrivial relation between laser phase and detector time $\zeta(\varphi)$. Physically, it is an ordinary time-dependent Doppler shift, and, hence, it non-linearly “stretches” the pulse of emitted radiation. The second effect is an amplitude damping due to the denominator in (13). To make things more clear we discuss these two effects separately before proceeding to analyze the spectral properties of the back-scattered radiation.

1. Detector time stretching

From the physical point of view the term $\int_0^\varphi a(\xi)^2 d\xi$ in (12) means that the electron rides the laser wave, so, during the interaction one observes a Doppler red-shifted signal on the detector. Hence, looking at the detected signal, one can say, that the initial pulse is “stretched” during the interaction. Fig. 1 illustrates this process. Here color-coded surface reproduces $A^L(\varphi)$ dependence with trivial dependence on ζ . The intersection of this surface with $\zeta(\varphi)$ provides “stretched” pulse when projected on (A, ζ) plane. The oscillations on $\zeta(\varphi)$ curve in case of linearly polarized pulse are discussed below.

Formally, the ponderomotive term $\int^\varphi a^2(\xi) d\xi$ is nothing else, but smooth non-decreasing function which asymptotically equals to zero at $\varphi = 0$ and some constant at $\varphi \rightarrow \pm\infty$. It can be thought of as a smooth approximation for the step function. For example, for the Gaussian pulse it will be equal to an error function plus a constant. If the amplitude is slow-varying, one can see the obvious consequence: the scattered pulse will have a chirp due

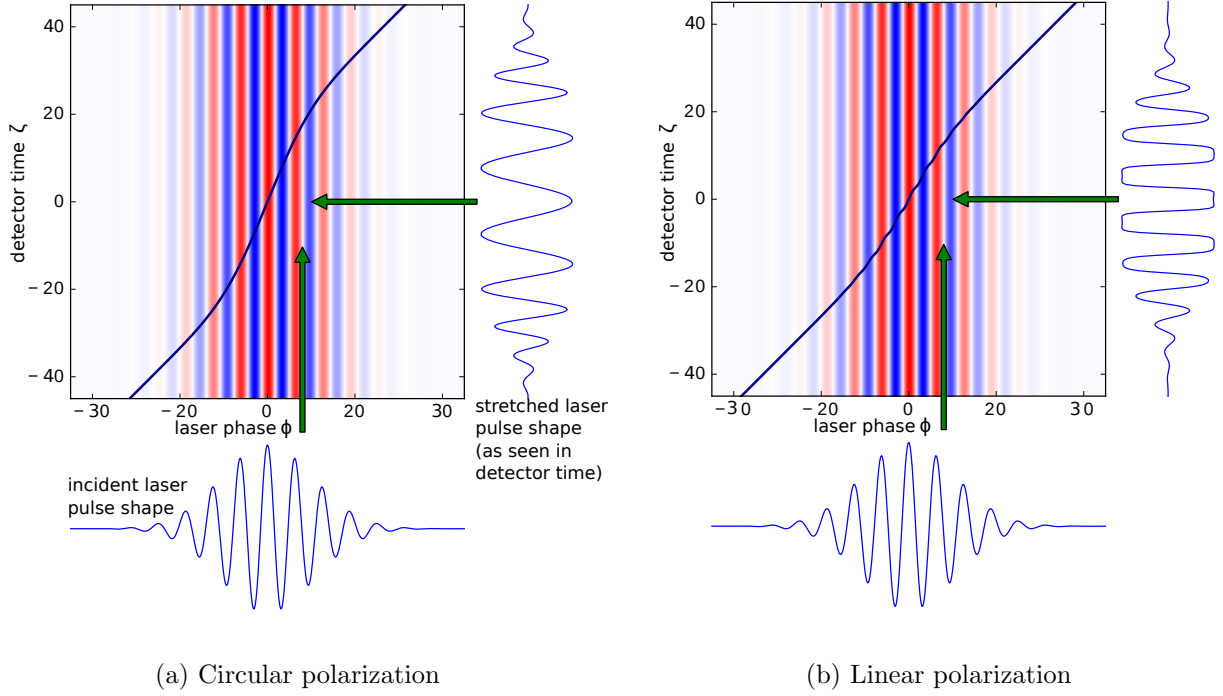


FIG. 1. $A^L(\varphi)$ is the color-coded surface. Dark line presents the $\zeta(\varphi)$ dependence (12). Projection of the surface section by $\zeta(\varphi)$ on ζ axis yields $A^L(\zeta)$.

to the factor of $\cos \varphi(\zeta)$ in the scattered vector-potential (that means, that the scattered frequency will vary with time), which will follow the shape of the incident pulse intensity.

2. Amplitude modulation

Here, we shall focus on the envelope of the scattered pulse without dealing with the pulse stretching. As has been mentioned before, for $a_0^2 \ll 1$ the envelope deformation can be neglected. When the amplitude grows, one must take the denominator of (13) into account. The amplitude of the field undergoes the following transformation

$$f : x \mapsto \frac{x}{1 + x^2}. \quad (14)$$

It is easy to see that it has a maximum at $x = 1$. This means the maximum amplitude of the scattered vector potential will be achieved when the instantaneous amplitude of the pulse is $a = 1$. The amplitude of light scattered by those parts of the laser pulse with an amplitude exceeding this value will be suppressed. It is also notable, that if the incoming pulse has a single peak with $a_0 > 1$ in time domain, the scattered pulse will break in two separate

peaks. The frequency of the emitted radiation around the maxima can be estimated as $\omega = 1/(1 + a^2) \approx 1/2$. The higher the pulse intensity, the larger is the separation of the peaks. In the limit of a high instantaneous value of $a \gg 1$, the damping of vector potential is proportional to a^{-1} . Moreover, the time stretching is proportional to a^2 . That is, the electric field of the scattered radiation will scale as a^{-3} , and the corresponding spectral intensity (see below) drops with a . In the limit of low $a \ll 1$, the intensity of the scattered radiation just scales as a^2 . Therefore, in the case of the laser pulses with high amplitude a_0 , we expect the spectral intensity of the scattered light to have a pronounced maximum at relatively high frequency arising from the scattering at the front and tail of the pulse.

3. Spectral intensity of the back-scattered light

For the non-negative frequencies the Fourier transform of the scattered vector potential is given by

$$A_x(\omega) = \frac{1}{2R} \int_{-\infty}^{\infty} a(\varphi) e^{i\omega\zeta - i\varphi} d\varphi. \quad (15)$$

For the frequencies in the range $\frac{1}{1+a_0^2} < \omega < 1$, the exponential factor in (15) has two stationary phase points[23, 31]. From now on, symmetric laser pulses centered in the origin are considered to simplify formulas, though the same can be done for asymmetric pulses as well. Using the stationary phase approximation, the integral in the r.h.s. of Eq. (15) can be represented in the following way:

$$A_x(\omega) \approx \frac{1}{R} \sqrt{\frac{2\pi}{\omega |(\ln a(\varphi_\omega)^2)'|}} \cos \left(\omega \int_0^{\varphi_\omega} (a(\xi)^2)' \xi d\xi + \frac{\pi}{4} \right), \quad (16)$$

where the stationary phase point φ_ω is defined by the following condition

$$\omega = \frac{1}{1 + a(\varphi_\omega)^2}, \quad (17)$$

$$\varphi_\omega > 0. \quad (18)$$

The divergence of the spectrum in the low-frequency edge is a result of the degeneracy of the corresponding stationary phase point. Much better agreement in the low-frequency tail can be obtained in terms of the Airy function[23, 31], but this is beyond the scope of this work. The spectral intensity is then given by[34, 36]

$$\left. \frac{d^2 I}{d\omega d\Omega} \right|_{\text{on-axis}} = \frac{\omega^2 R^2}{\pi^2} |A_x(\omega)|^2, \quad (19)$$

where $d\Omega$ stands for solid angle element. In writing this expression, both x and y components were taken into account as they provide exactly the same spectral intensity.

To extract the scaling of the spectrum with peak value of field and duration it is convenient to introduce the normalized pulse intensity profile f and pulse duration τ :

$$a(\varphi)^2 = a_0^2 f(\varphi/\tau), \quad (20)$$

$$f(0) = 1. \quad (21)$$

The expression for the intensity distribution transforms to

$$\left. \frac{d^2 I}{d\omega d\Omega} \right|_{\text{on-axis}} = \frac{2\omega\tau}{\pi} \left| y \frac{df^{-1}(y)}{dy} \right| \cos^2 \chi, \quad (22)$$

where

$$\chi = \omega\tau a_0^2 \int_y^1 f^{-1}(\xi) d\xi - \frac{\pi}{4}, \quad (23)$$

$$y = \frac{1 - \omega}{a_0^2 \omega}, \quad (24)$$

$$0 < y < 1. \quad (25)$$

Here, the non-negative inverse function f^{-1} of the normalized pulse intensity profile f is taken. In Eq. (22), the squared cosine factor defines the interference structure in the non-linear TS spectrum, and the prefactor defines the envelope of the spectrum. The cosine argument can be interpreted as the optical path difference for the light emitted at the pulse front and at the pulse tail at the same intensity level. The number of interference fringes can be estimated as $\tau a_0^2 / \pi$ [23]. Here, one sees that the pulse duration does not affect the average shape of the spectrum, but only the overall scaling and the frequency of the interference fringes. One can also notice, that due to the factor df^{-1}/dy , a steep envelope of the incident pulse will provide less energy in the back-scattered pulse in comparison with a gradual one.

C. Linear polarization

One can apply the machinery developed in the previous subsection also to linear polarization of the incident pulse with the vector potential in the following form

$$A_x^L(\varphi) = a(\varphi) \cos \varphi. \quad (26)$$

$$A_y^L(\varphi) = 0. \quad (27)$$

Equation (8) for the vector potential of the scattered light then can be rewritten as

$$A_x(\zeta) = \frac{1}{R} \frac{a(\varphi(\zeta)) \cos(\varphi(\zeta))}{1 + a(\varphi(\zeta))^2 \cos(\varphi(\zeta))^2}. \quad (28)$$

$$\zeta = \varphi + \int_0^\varphi a(\xi)^2 \cos(\xi)^2 d\xi. \quad (29)$$

Here, the detector time ζ has rapidly oscillating components as a function of the laser phase φ . This is because for linear polarization the electron oscillates longitudinally along the z -axis. The retardation between laser phase and detector time also oscillates, and the oscillations cause the appearance of the high order harmonics in the scattered spectrum (see Fig 1b).

The Fourier transform of Eq. (28) yields

$$A_x(\omega) = \frac{1}{R} \int_{-\infty}^{+\infty} e^{i\omega\zeta} a(\varphi) \cos \varphi d\varphi. \quad (30)$$

Note that unlike Eq. (15) one has to keep the cosine without passing to a complex amplitude in this expression because of the oscillatory part in the exponential. Now, one may want to eliminate the oscillations in the exponent, arising due to the cosine term in the expression (29) for ζ . Assuming, that the laser pulse amplitude is slow-varying, one can write

$$\zeta \approx \varphi + \frac{1}{4}a(\varphi)^2 \sin 2\varphi + \frac{1}{2} \int_0^\varphi a(\xi)^2 d\xi. \quad (31)$$

As was done in the previous section, one can introduce the normalized intensity profile (20) and perform the integration using the stationary phase approximation. Doing so results in

$$A_x(\omega) \approx \sum_{m=2k+1} (-1)^{\frac{m-1}{2}} \sqrt{\frac{4\pi\tau}{R^2\omega} \left| y \frac{df^{-1}}{dy} \right|_{y_m}} P_m \left(\frac{m-\omega}{2} \right) \cos \chi_m. \quad (32)$$

$$P_m(x) = J_{\frac{m-1}{2}}(x) - J_{\frac{m+1}{2}}(x), \quad (33)$$

$$\chi_m = \frac{\omega\tau a_0^2}{2} \int_{y_m}^1 f^{-1}(\xi) d\xi - \frac{\pi}{4}, \quad (34)$$

$$y_m = 2 \frac{m-\omega}{a_0^2\omega}. \quad (35)$$

Here J_m is the Bessel function of m -th order. Note, that for the calculation of the contribution of m -th harmonic, the stationary phase approximation requires $\omega \in \left(\frac{m}{1+a_0^2/2}, m\right)$. From here it follows, that the harmonics start overlapping in the spectral domain for $m \geq 2/a_0^2$.

For the non-interfering part of the spectrum one can write

$$\left.\frac{d^2 I_m}{d\omega d\Omega}\right|_{\text{on-axis}} = \frac{2\omega\tau}{\pi} \left|y_m \frac{df^{-1}(y_m)}{dy_m}\right| P_m^2 \left(\frac{m-\omega}{2}\right) \cos^2 \chi_m, \quad (36)$$

where m is an odd number. One can see, that the shape of each particular harmonic is similar to the case of a circularly polarized pulse. The only difference is the factor P_m containing the Bessel functions. The argument of Bessel functions ranges from $\frac{ma_0^2}{2+a_0^2}$ to 0 with increasing frequency. Knowing that $J_\alpha(x) \sim x^\alpha$, one can conclude, that this factor will lead to the suppression of high frequencies inside every harmonic except the first one. Decrease of the maximum value of $J_\alpha(x)$ with α provides the suppression of high-order harmonic emission in general.

In this section we have analyzed the time-dependence of the scattered vector potential in the nonlinear TS. The complete analytical expressions for the spectral intensity of the back-scattered radiation have been written in the stationary phase approximation. Now we turn to the numerical evaluation of the spectra and comparison between exact and approximate solutions.

III. NUMERICAL CALCULATIONS

A. Method

Since the expression for the scattered vector potential (8) is exact, there is essentially no need to numerically solve the equations of motion for calculation of the back-scattered spectrum. This allows us to greatly simplify the entire calculation process. The routine for calculating the back-scattered spectrum for any given incident laser pulse is the following:

- Using ordinary integration routines (either numerical, or analytical), one obtains the $\zeta(\varphi)$ dependence. In the case of evenly distributed discrete points $\{\varphi_i\}$, this results in the discrete set of corresponding detector times $\{\zeta_i(\varphi_i)\}$. As discussed in Sec. II B 1, the $\{\zeta_i\}$ points will be distributed unevenly.

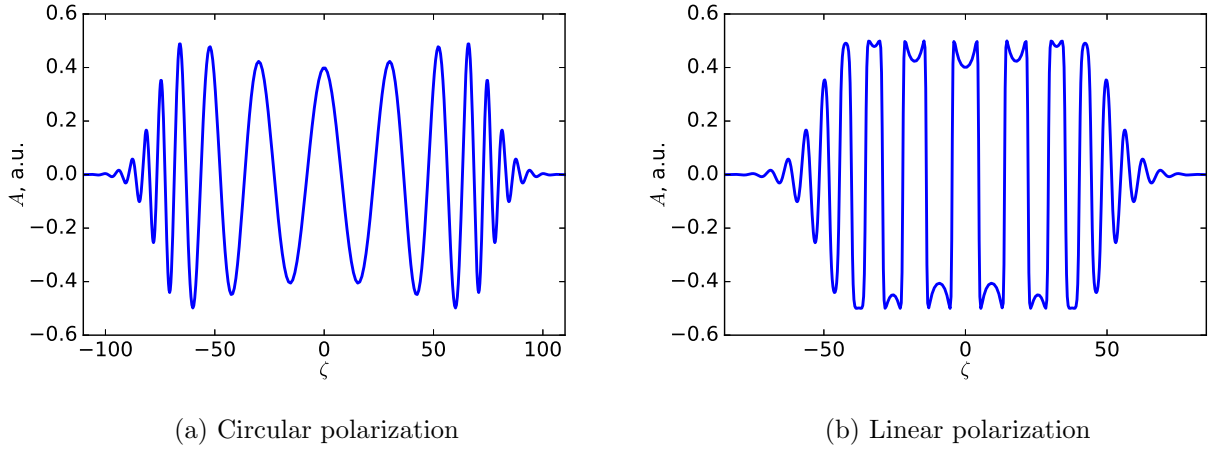
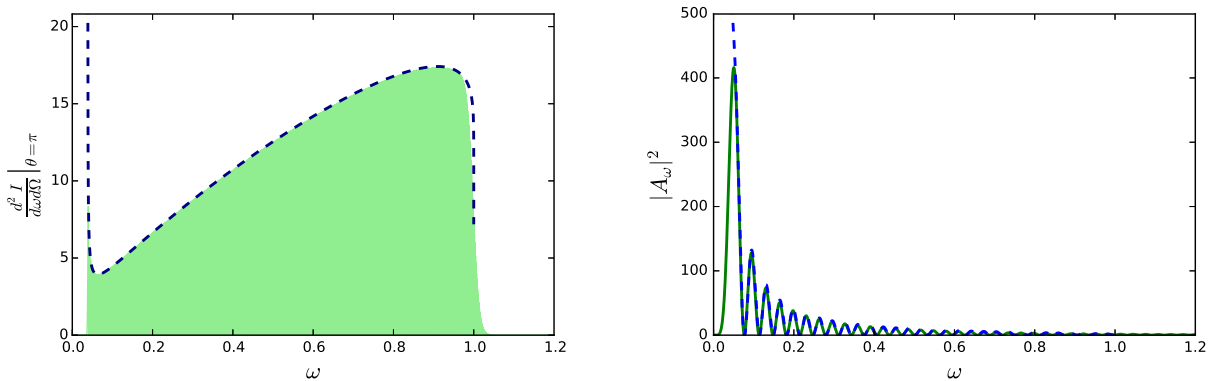


FIG. 2. Temporal structure of the scattered pulse. The incident pulse has Gaussian envelope, $a_0 = 2$, $\tau = 20$.

- The scattered field value at each point φ_i is found using Eq. (8). As a result, one obtains the scattered pulse vector-potential in the temporal domain $\{(\zeta_i, A_i)\}$ (Figs. 1, 2).
- Discrete dependence $\{(\zeta_i, A_i)\}$ is Fourier transformed. In most cases, values of ζ_i will be distributed unevenly, so to make this step effective one can either use the Fast Fourier Transform (FFT) routines in combination with interpolation, or special techniques of discrete Fourier transform on unevenly spaced grids. In what follows the first option (interpolation) was used. At this point one can notice that using detector time improves performance of the computations. Namely, the number of operations needed to calculate on-axis spectrum using ordinary integration routines scales as $O(N^2)$ with N being the number of points on the trajectory, while using detector time allows using FFT directly. Interpolation scales as $O(N)$, and FFT as $O(N \log N)$. Therefore, overall number of operations scales as $O(N \log N)$.

B. Results

From now on, we assume the case of circularly polarized light. Consider three types of the pulse shapes, namely cosine, cosine-squared and Gaussian (see Appendix B for details). For sufficiently long pulses (with duration $\tau \gg 1$), the stationary phase approximation yields



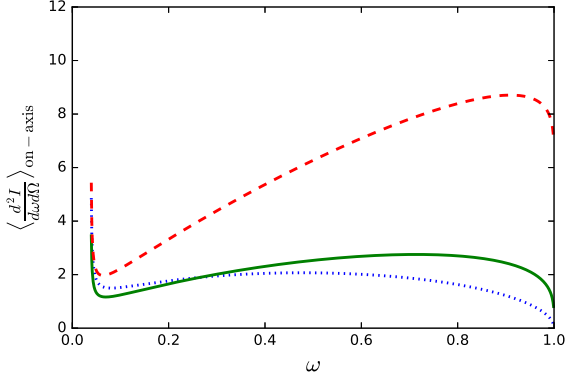
(a) Spectral intensity of the back-scattered light. (b) Squared absolute spectrum of the vector-potential

Analytical result presents spectral envelope. Incident pulse has cosine envelope, $a_0 = 5$, $\tau = 200$. Incident pulse has Gaussian envelope, $a_0 = 5$, $\tau = 20$.

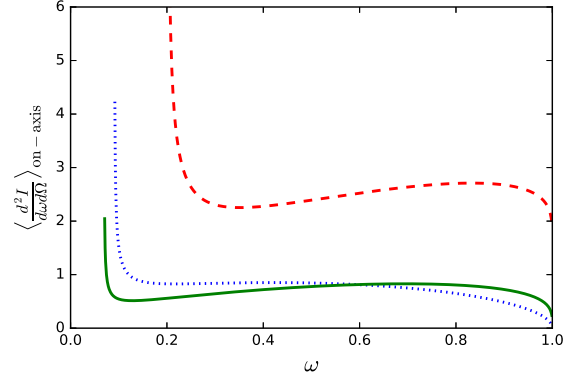
FIG. 3. Comparison between results of numerical simulations (solid) and stationary phase approximation (dashed).

very good agreement with the results of the numerical calculations. It describes both the spectral envelope (Fig. 3a) and the interference structure (Fig. 3b). In the most part of described frequency region $\omega \in (\frac{1}{1+a_0^2}, 1)$, the approximation is applicable. Note, that the numerical result fills the area on Fig. 3a due to dense interference structure for the high values of peak intensity and duration used in this example ($a_0 = 5$, $\tau = 200$). Figure 3b presents the situation where the pulse duration is lower, hence, the interference structure is more distinguishable. There is one more notable thing about the spectrum on Fig. 3a - the peak of the spectral envelope at relatively high frequencies. The origin of this peak was discussed in Sec. II B 2.

The subject of great interest is the influence of the pulse shape on the spectrum of the back-scattered radiation. Considering the incident pulse having slowly varying amplitude, one can use equation (22) to obtain the average spectrum of the scattered pulse. The average spectral intensity directly includes the shape of the pulse. Hence, different pulse shapes with the same peak intensity yield significantly different spectral intensity profiles (Fig. 4a). The huge discrepancy between light scattered by Gaussian pulse and cos-pulses is due to fact that Gaussian pulse has wide, smooth low-intensity wings in contrast to the finite support pulses. These wings provide efficient back-scattering at relatively high frequencies, while the



(a) $a_0 = 5$, $\tau = 100$.



(b) $\int a'(\varphi)^2 d\varphi = 250$, $\tau = 50$.

FIG. 4. Average spectral intensity of the back-scattered radiation. Fixed peak field value (a) and fixed incident pulse energy (b). Incident pulse has cosine-squared (solid), Gaussian (dashed) and cosine (dotted) envelope. The analytic expressions are collected in B.

low-frequency part of the spectrum is relatively suppressed.

Assuming the incident pulse to be symmetric, one can directly reconstruct the pulse shape from the average spectral intensity profile, up to the pulse duration. The value of a_0 can be extracted from the low frequency cutoff, and the envelope itself. Knowing a_0 , using (22) one can obtain the $f^{-1}(y)$ dependence, hence the temporal laser intensity profile. One can also see that the differences in the scattering picture occur in the case of the fixed incident pulse energy as well (Fig. 4b). This finding can be used in high intensity laser-matter interactions experiments for laser pulse characterization. This scheme, of course, requires circular polarization as for linear polarization different harmonics are overlapping and the shape of the first harmonic cannot be determined.

IV. CONCLUSIONS

In this paper the nonlinear Thomson back-scattering was studied within the classical framework. It has been shown that interpretation of $\zeta = t + z$ variable as the detector time significantly simplifies the calculation of the scattered radiation. It also leads to the simple way of analytical description of the scattered spectra. Temporal properties of the light scattered on the single electron allow one to make qualitative conclusions about the spectrum which stay true if the scattering occurs on many particles incoherently. Using this

approach, we compared the back-scattered spectra for various pulse shapes, and came to the conclusion that the pulse shape strongly affects the scattered spectrum. Under some assumptions (symmetric pulse peak, high peak intensity and relatively high duration) pulse shape can be reconstructed from the scattered spectral intensity, even if the interference structure is not resolved.

We have not discussed the spectrum modification due to initial velocity spread of the electrons, which definitely affects the back-scattered spectrum. This effect can also be significant and can be the subject of further investigation.

ACKNOWLEDGMENTS

This work was supported by the Helmholtz Association (Helmholtz Young Investigators group VH-NG-1037).

Appendix A: Derivation of Eq. (32)

Assuming the amplitude to be slowly varying one can start with the expression

$$A_x(\omega) = \frac{1}{2R} \int_{-\infty}^{+\infty} (e^{i(\omega+1)\varphi} + e^{i(\omega-1)\varphi}) a(\varphi) \exp \left(\frac{i\omega}{4} a(\varphi)^2 \sin 2\varphi + \frac{i\omega}{2} \int_0^\varphi a(\xi)^2 d\xi \right) d\varphi. \quad (\text{A1})$$

Using the Jacobi-Anger expansion

$$\exp \left(\frac{i\omega}{4} a(\varphi)^2 \sin 2\varphi \right) = \sum_{m=-\infty}^{\infty} J_m \left(\frac{\omega a(\varphi)^2}{4} \right) e^{2im\varphi}, \quad (\text{A2})$$

one can rewrite this integral as a sum over harmonics:

$$A_x(\omega) = \frac{1}{2R} \sum_{m=-\infty}^{\infty} \int_{-\infty}^{+\infty} \left(J_m \left(\frac{\omega a^2}{4} \right) + J_{m+1} \left(\frac{\omega a^2}{4} \right) \right) a(\varphi) e^{i(\omega+2m-1)\varphi + \frac{i\omega}{2} \int a^2 d\xi} d\varphi. \quad (\text{A3})$$

Now one can apply the stationary phase approximation and notice that for each term the stationary point condition is $\omega = \frac{1-2m}{1+a^2/2}$:

$$A_x(\omega) \approx \sum_{m=-\infty}^{\infty} \sqrt{\frac{4\pi a^2}{R^2 \omega (a^2)'}} \left(J_m \left(\frac{\omega a^2}{2} \right) + J_{m-1} \left(\frac{\omega a^2}{4} \right) \right) \cos \left((\omega + 2m + 1)\varphi^* + \frac{\omega}{2} \int_0^{\varphi^*} a^2 d\xi - \frac{\pi}{4} \right), \quad (\text{A4})$$

TABLE I. Pulse shapes and corresponding stationary point average spectra

Name used in text	$a(\varphi)$	$f(x)$	$\langle \frac{d^2 I}{d\omega d\Omega} \rangle_{\text{on-axis}}$
Gaussian	$a_0 \exp\left(-\frac{\varphi^2}{\tau^2}\right)$	e^{-2x^2}	$\frac{\omega_T}{4\pi} \left(\frac{1}{2} \ln \frac{a_0^2 \omega}{1-\omega}\right)^{-1/2}$
cosine	$\begin{cases} a_0 \cos \frac{\pi\varphi}{\tau}, & \varphi \in [-\frac{\tau}{2}, \frac{\tau}{2}] \\ 0 & \text{otherwise} \end{cases}$	$\begin{cases} \cos^2 \pi x, & x \in [-\frac{1}{2}, \frac{1}{2}] \\ 0 & \text{otherwise} \end{cases}$	$\frac{\omega_T}{\pi^2} \left(\frac{a_0^2 \omega}{1-\omega} - 1\right)^{-1/2}$
cosine-squared	$\begin{cases} a_0 \cos^2 \frac{\pi\varphi}{\tau}, & \varphi \in [-\frac{\tau}{2}, \frac{\tau}{2}] \\ 0 & \text{otherwise} \end{cases}$	$\begin{cases} \cos^4 \pi x, & x \in [-\frac{1}{2}, \frac{1}{2}] \\ 0 & \text{otherwise} \end{cases}$	$\frac{\omega_T}{2\pi^2} \left(\sqrt{\frac{a_0^2 \omega}{1-\omega}} - 1\right)^{-1/2}$

where $\varphi^* > 0$ is the value obtained from the stationary phase condition. Changing summation index to $1 - 2m$ and substituting φ^* provides now Eq. (32).

Appendix B: Scattered spectrum for particular pulse shapes

In the calculations of the average spectral intensity three different pulse shapes were used. For all pulses considered, corresponding expressions can be obtained analytically using (22). The descriptions of pulse shapes and average scattered spectra for circularly polarized light are presented in Table I.

-
- [1] E. Esarey, S. K. Ride, and P. Sprangle, Phys. Rev. E **48**, 3003 (1993).
 - [2] W. Leemans, R. Schoenlein, P. Volfbeyn, A. Chin, T. Glover, P. Balling, M. Zolotarev, K. Kim, S. Chattopadhyay, and C. Shank, Physical review letters **77**, 4182 (1996).
 - [3] F. Albert, S. G. Anderson, D. J. Gibson, C. A. Hagmann, M. S. Johnson, M. Messerly, V. Semenov, M. Y. Shverdin, B. Rusnak, A. M. Tremaine, F. V. Hartemann, C. W. Siders, D. P. McNabb, and C. P. J. Barty, Physical Review Special Topics - Accelerators and Beams **13**, 070704 (2010).
 - [4] V. Karagodsky and L. Schächter, Plas. Phys. and Controlled Fusion **53**, 014007 (2011).
 - [5] S. G. Rykovanov, C. G. R. Geddes, J.-L. Vay, C. B. Schroeder, E. Esarey, and W. P. Leemans, J. Phys. B **47**, 234013 (2014).
 - [6] K. Khrennikov, J. Wenz, A. Buck, J. Xu, M. Heigoldt, L. Veisz, and S. Karsch, Physical Review Letters **114**, 195003 (2015).

- [7] G. Sarri, D. Corvan, W. Schumaker, J. Cole, A. Di Piazza, H. Ahmed, C. Harvey, C. H. Keitel, K. Krushelnick, S. Mangles, *et al.*, Physical review letters **113**, 224801 (2014).
- [8] N. D. Powers, I. Ghebregziabher, G. Golovin, C. Liu, S. Chen, S. Banerjee, J. Zhang, and D. P. Umstadter, Nature Photonics **8**, 28 (2014).
- [9] V. G. Nedorezov, A. A. Turinge, and Y. M. Shatunov, Physics-Uspekhi **47**, 341 (2004).
- [10] P. Thirolf, L. Csige, and D. Habs, EPJ Web Conf. **38**, 08001 (2012).
- [11] O. Tesileanu, D. Ursescu, R. Dabu, and N. V. Zamfir, J. Phys. Conf. Ser. **420**, 012157 (2013).
- [12] M. S. Johnson, J. M. Hall, D. P. McNabb, M. J. Tuffley, M. W. Ahmed, S. Stave, H. R. Weller, H. Karwowski, J. Thompkins, F. D. McDaniel, and B. L. Doyle, AIP Conf. Proc. **590**, 590 (2011).
- [13] K. Weeks, V. Litvinenko, and J. Madey, Med. Phys. **24**, 417 (1997).
- [14] R. Tommasini, S. P. Hatchett, D. S. Hey, C. Iglesias, N. Izumi, J. A. Koch, O. L. Landen, A. J. MacKinnon, C. Sorce, J. A. Delettrez, V. Y. Glebov, T. C. Sangster, and C. Stoeckl, Phys. Plas. **18**, 056309 (2011).
- [15] H. Toyokawa, H. Ohgaki, T. Mikado, and K. Yamada, Review of Scientific Instruments **73**, 3358 (2002).
- [16] W. Bertozzi, J. Caggiano, W. Hensley, M. Johnson, S. Korbly, R. Ledoux, D. McNabb, E. Norman, W. Park, and G. Warren, Phys. Rev. C **78**, 041601 (2008).
- [17] B. J. Quiter, B. A. Ludewigt, V. V. Mozin, and S. G. Prussin, IEEE Transactions on Nuclear Science **58**, 400 (2011).
- [18] C. G. Geddes, S. Rykovanov, N. H. Matlis, S. Steinke, J.-L. Vay, E. H. Esarey, B. Ludewigt, K. Nakamura, B. J. Quiter, C. B. Schroeder, C. Toth, and W. P. Leemans, Nucl. Instr. Methods Phys. Res. Sect. B **350**, 116 (2015).
- [19] F. V. Hartemann, A. L. Troha, N. C. Luhmann Jr., and Z. Toffano, Phys. Rev. E **54**, 2956 (1996).
- [20] C. Brau, Phys. Rev. ST – Accel. Beams **7**, 020701 (2004).
- [21] G. A. Krafft, Phys. Rev. Lett. **92**, 204802 (2004).
- [22] F. Mackenroth and A. Di Piazza, Phys. Rev. A **83**, 032106 (2011).
- [23] D. Seipt and B. Kämpfer, Laser Phys. **23**, 75301 (2013).
- [24] D. Seipt and B. Kämpfer, Phys. Rev. A **83**, 22101 (2011).

- [25] S. G. Rykovanov, C. G. R. Geddes, C. B. Schroeder, E. Esarey, and W. P. Leemans, “Controlling the spectral shape of nonlinear Thomson scattering with proper laser chirping,” (2014), arXiv:1412.2517 [physics.plasma-ph].
- [26] I. Ghebregziabher, B. A. Shadwick, and D. Umstadter, Phys. Rev. ST Accel. Beams **16**, 30705 (2013).
- [27] B. Terzić, K. Deitrick, A. S. Hofer, and G. A. Krafft, Phys. Rev. Lett. **112**, 074801 (2014).
- [28] D. Seipt, S. G. Rykovanov, A. Surzhykov, and S. Fritzsche, Phys. Rev. A **91**, 033402 (2015).
- [29] A. Liénard, L’Éclairage électrique : revue hebdomadaire d’électricité **XVI**, 5 (1898).
- [30] E. Wiechert, Annalen der Physik **309**, 667 (1901).
- [31] N. B. Narozhnyi and M. S. Fofanov, J. Exp. Theor. Phys. **83**, 14 (1996).
- [32] K. Krajewska and J. Z. Kamiński, Laser and Particle Beams **31**, 503 (2013).
- [33] K. Krajewska and J. Z. Kamiński, Phys. Rev. A **90**, 052117 (2014).
- [34] L. Landau and E. Lifshitz, *The Classical Theory of Fields, Fourth Edition: Volume 2 (Course of Theoretical Physics Series)*, 4th ed. (Butterworth-Heinemann, 1980).
- [35] T. Heinzl, D. Seipt, and B. Kämpfer, Phys. Rev. A **81**, 022125 (2010).
- [36] J. D. Jackson, *Classical electrodynamics*, Vol. 3 (Wiley New York etc., 1962).